Human Molecular Genetics, 2014, Vol. 23, No. 4 **843–854**
doi:10.1093/hmg/ddt468
Advance Access published on September 24, 2013

Neuronal accumulation of glucosylceramide in a mouse model of neuronopathic Gaucher disease leads to neurodegeneration

Tamar Farfel-Becker[1], Einat B. Vitner[1], Samuel L. Kelly[3], Jessica R. Bame[3], Jingjing Duan[3], Vera Shinder[2], Alfred H. Merrill, Jr[3], Kostantin Dobrenis[4] and Anthony H. Futerman[1,*]

[1]Departments of Biological Chemistry and [2]Chemical Research Support, Weizmann Institute of Science, Rehovot 76100, Israel [3]School of Biology and Petit Institute for Bioengineering and Bioscience, Georgia Institute of Technology, Atlanta, USA [4]Dominick P. Purpura Department of Neuroscience, Albert Einstein College of Medicine of Yeshiva University, Bronx, NY, USA

Received July 29, 2013; Revised and Accepted September 19, 2013

Gaucher disease has recently received wide attention due to the unexpected discovery that it is a genetic risk factor for Parkinson's disease. Gaucher disease is caused by the defective activity of the lysosomal enzyme, glucocerebrosidase (GCase; GBA1), resulting in intracellular accumulation of the glycosphingolipids, glucosylceramide and psychosine. The rare neuronopathic forms of GD (nGD) are characterized by profound neurological impairment and neuronal cell death. We have previously described the progression of neuropathological changes in a mouse model of nGD. We now examine the relationship between glycosphingolipid accumulation and initiation of pathology at two pre-symptomatic stages of the disease in four different brain areas which display differential degrees of susceptibility to GCase deficiency. Liquid chromatography electrospray ionization tandem mass spectrometry demonstrated glucosylceramide and psychosine accumulation in nGD brains prior to the appearance of neuroinflammation, although only glucosylceramide accumulation correlated with neuroinflammation and neuron loss. Levels of other sphingolipids, including the pro-apoptotic lipid, ceramide, were mostly unaltered. Transmission electron microscopy revealed that glucosylceramide accumulation occurs in neurons, mostly in the form of membrane-delimited pseudo-tubules located near the nucleus. Highly disrupted glucosylceramide-storing cells, which are likely degenerating neurons containing massive inclusions, numerous autophagosomes and unique ultrastructural features, were also observed. Together, our results indicate that a certain level of neuronal glucosylceramide storage is required to trigger neuropathological changes in affected brain areas, while other brain areas containing similar glucosylceramide levels are unaltered, presumably because of intrinsic differences in neuronal properties, or in the neuronal environment, between various brain regions.

INTRODUCTION

Gaucher disease (GD), the most common lysosomal storage disease (LSD) (1,2), is an inherited recessive metabolic disorder caused by mutations in acid-β-glucosidase (glucocerebrosidase, GCase, GBA1) (3), the lysosomal enzyme that cleaves the glycosphingolipid (GSL), glucosylceramide (D-glucosyl-β1-1′-*N*-acyl-D-*erythro*-sphingosine; GlcCer), to ceramide and glucose. GD patients are classified into three clinical sub-types; type 1 is the chronic, non-neuronopathic form (3) and types 2 and 3 are the acute (4,5) and chronic (6) neuronopathic (nGD) forms which display central nervous system (CNS) involvement in addition to systemic disease. An unexpected association between mutations in the GBA1 gene and Parkinson's disease has been recognized recently, in which GD carriers are predisposed towards the development of Parkinson's disease (7). While type 1 GD patients can be successfully treated with enzyme replacement therapy, there is currently no effective treatment for the neurological signs of the disease as the recombinant enzyme does not cross the blood–brain–barrier (8,9).

*To whom correspondence should be addressed. Tel: +972 89342704; Fax: +972 89344112; Email: tony.futerman@weizmann.ac.il

GlcCer and its deacylated form, psychosine (D-glucosyl-β1-1′-D-*erythro*-sphingosine; glucosylsphingosine), accumulate in the brain in both nGD patients (10,11) and in nGD mice (12–14). It has been suggested that psychosine accumulation is the primary event leading to brain pathology in nGD (10,13,15,16), but a systematic evaluation of the contribution of psychosine and GlcCer to the initiation of pathological changes in the nGD brain has not been performed. GlcCer storage in the brain was reported to occur mainly in perivascular macrophages, and GlcCer storage within neurons has been considered rare (11,17,18).

We previously described (19) the progression of neuropathological changes in an nGD mouse model (the $Gba^{flox/flox}$; nestin-Cre mouse) (20), and demonstrated that neuroinflammation (i.e. microglial activation and astrogliosis) is an early event in disease progression, appearing prior to disease manifestation, and is tightly correlated with neuron loss (19,21). Interestingly, these pathological events occur in specific brain areas (such as cortical layer V, also shown to be affected in human nGD brain) (22), while other brain areas remain unaffected even at late stages of the disease (19). We now use two independent techniques, namely liquid chromatography electrospray ionization tandem mass spectrometry (LC-ESI-MS/MS) and transmission electron microscopy, to assess the relationship between GSL accumulation and neuropathology. Our data are consistent with the notion that upon reaching a threshold of GlcCer accumulation, but not of psychosine, certain brain areas display neuropathology due to intrinsic properties of these specific brain areas rather than due to differential levels of GlcCer accumulation, and that neuronal GlcCer storage is a critical determinant of neuronal cell demise.

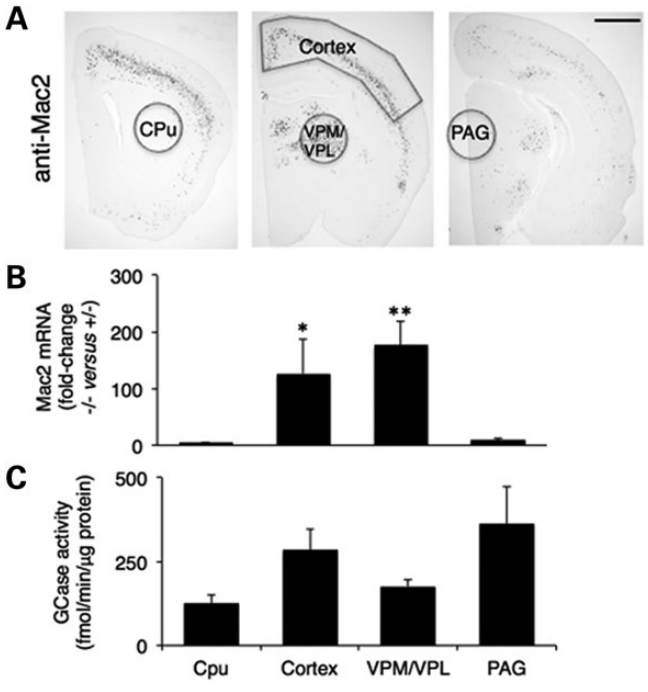

Figure 1. Characterization of brain areas used in this study. (**A**) Immunohistochemical labeling for Mac2 on coronal brain sections from 16-day-old −/− mice. Brain areas that were subsequently used for biochemical analysis are indicated. No staining was observed in control brains. Scale bar = 1 mm. (**B**) Quantitative PCR analysis of Mac2 mRNA in different brain areas of 14-day-old mice. Values are means ± s.e.m, $n = 5$. $^{*}P < 0.05$, $^{**}P < 0.01$. (**C**) GCase activity in nGD brains. Values are means ± s.e.m., $n = 3$.

RESULTS

Sphingolipid profile of the nGD brain

We first examined sphingolipid (SL) levels in different brain areas to determine the relationship between changes in SL levels and the development of neuropathology. Brain areas were chosen based on the extent of pathology (Fig. 1A) (19), which was quantified by mRNA expression of the microglial marker, Mac2 (Fig. 1B), previously shown to correlate with astrogliosis and neuron loss (19), and on levels of residual GCase activity (Fig. 1C). Two areas, namely the cortex and the ventral posteromedial/posterolateral (VPM/VPL) region of the thalamus were designated as areas displaying significant pathology, whereas the caudate putamen (CPu) and the periaqueductal gray (PAG) were designated as areas that did not display pathology (Fig. 1A). These regions were dissected out such that their area did not exceed $1 \times 1\ mm^2$ (apart from the cortex, which was peeled away using a spatula) (Fig. 1A). Residual levels of GCase activity were similar in all four areas of the −/− mouse (Fig. 1C) and were ∼10- to 20-fold lower than in +/− mice (GCase activity levels in +/− mice were ∼2–3 pmol/μg protein/min compared with 0.15–0.35 pmol/μg protein/min in −/− mice). No correlation was observed between the extent of Mac2-immunostaining or mRNA expression and levels of residual GCase activity (Fig. 1).

The SL profile of −/− and +/− mice was determined by LC-ESI-MS/MS in all four brain areas at two different ages, both of which are prior to disease overt manifestations [defined herein as the pre-symptomatic stage; see also (19)]: 10-day-old mice, in which no neuroinflammation is detected (19,21) and 14-day-old mice, which is soon after the appearance of the first indicators of neuroinflammation (19,21) but prior to the appearance of other pathological features (such as reduced brain weight and reduced cortical thickness) (19). Previous studies have shown that GlcCer and psychosine levels do not differ between +/− and +/+ mouse brains (13,20,23), even though GCase activity is reduced by ∼50% in the former (12).

SLs are composed of a sphingoid long chain base (normally sphingosine or sphinganine) to which a fatty acid is *N*-acylated (24); the length of the fatty acid varies between different SLs (25) and between different tissues (26,27), with brain containing particularly high levels of C18- and C24:1-SLs (28). Total levels of GlcCer (i.e. the sum of all of the GlcCer species containing different length fatty acids) were elevated 2- to 3-fold in 10-day-old −/− mice compared with +/− mice in the CPu, cortex and VPM/VPL, but not in the PAG (Fig. 2), with an elevation of 7- to 10-fold in 14-day-old mice in all areas except the PAG, in which GlcCer levels were elevated by ∼4-fold (Fig. 2). Some variation in GlcCer acyl chain length was observed in +/− mice, with a relatively high proportion of very-long chain GlcCer (C22, C24 and C24:1) in the VPM/VPL and PAG compared with the CPu and cortex at 10 days of age (Fig. 2), and a lower proportion of these species in the cortex of 14-day-old +/− mice (Fig. 2). The main GlcCer species that was elevated in −/− brain was C18-GlcCer, which displayed the earliest and most pronounced elevation. An elevation in very-long (C22-C24) acyl chain GlcCer was only apparent at 14 days of age (Table 1). There was no correlation between GlcCer levels

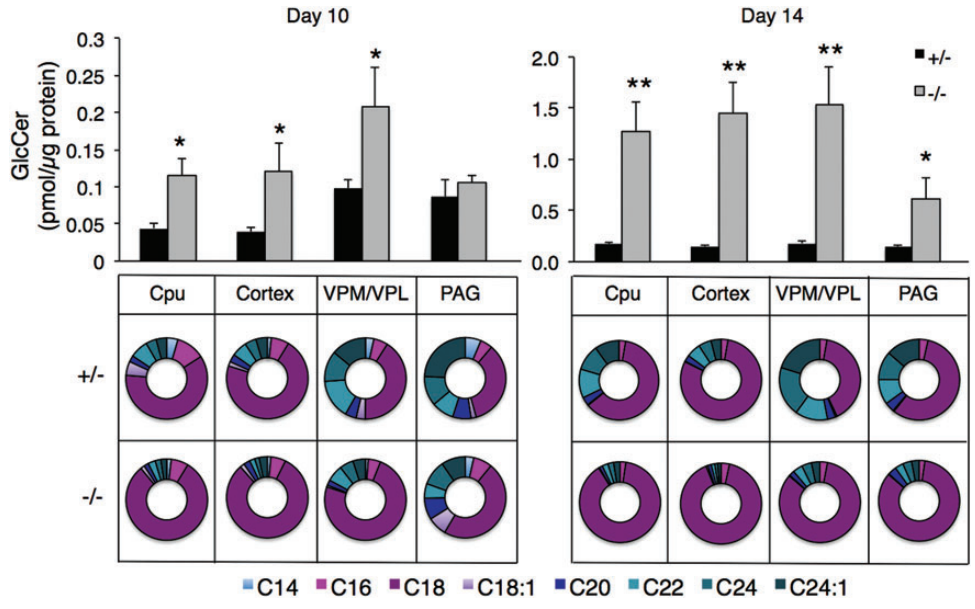

Figure 2. GlcCer levels and *N*-acyl chain species in nGD brains. Total GlcCer levels are shown in the upper panels and *N*-acyl chain length distribution in the bottom panels. Values are means ± s.e.m., $n = 4–5$. $^{*}P < 0.05$, $^{**}P < 0.01$.

and pathology, as the CPu, VPM/VPL and cortex showed similar levels of GlcCer accumulation, although pathology is apparent only in the latter two areas.

In contrast to the significant elevation in GlcCer levels between Days 10 and 14, only a small increase in psychosine levels was detected between these two ages (Fig. 3). Importantly, no changes in the extent of psychosine elevation were detected in the VPM/VPL between Days 10 and 14 (Table 2), even though pathology becomes very prominent in the VPM/VPL between these two ages (19). Moreover, total psychosine levels (0.01 ± 0.002 pmol/μg protein) in the VPM/VPL region of −/− mice are ∼140-fold less than those of GlcCer (1.54 ± 0.37 pmol/μg protein).

Apart from minor and sporadic differences, no significant changes in levels of other SLs were detected, including (i) ceramide (Fig. 4), a pro-apoptotic lipid that has been suggested to play a role in the association between GD and Parkinson's disease (29,30), (ii) lactosylceramide (LacCer) (Fig. 4), the sphingolipid up-stream to GlcCer in the GSL degradative pathway, (iii) galactosylceramide (GalCer) and (iv) sphingomyelin (SM) (Fig. 5). Minor changes were seen in the ceramide acyl chain length in the VPM/VPL of 14-day-old −/− mice (with C16-ceramide elevated by ∼2.5-fold, C18-ceramide elevated ∼1.4-fold and C20-ceramide elevated ∼1.4-fold), which might reflect changes in the cellular composition of this area due to infiltration and proliferation of immune cells (19). Some minor changes were also observed in the GalCer acyl chain length in the CPu (C16-GalCer was elevated ∼1.5-fold, C18-GalCer was elevated ∼1.9-fold) and in the cortex of 14-day-old −/− mice, in which C18-GalCer was elevated ∼1.5-fold. C16-SM was elevated in the cortex (∼1.3-fold) and in the VPM/VPL (∼1.8-fold elevation). Finally, no changes were detected in levels of the long chain bases sphingosine, sphinganine, sphingosine-1-phosphate and sphinganine-1-phosphate between +/− and −/− mice at 10 or 14 days of

Table 1. Fold-change of GlcCer species in different brain areas at different ages

GlcCer *N*-acyl chain length	10-day-old mice Ratio (−/− versus +/−)	*P*-value	14-day-old mice Ratio (−/− versus +/−)	*P*-value
CPu				
C16	3.0 ± 1.3	ns	6.9 ± 1.7	<0.01
C18	5.7 ± 1.8	<0.01	10.9 ± 2.6	<0.005
C18:1	1.6 ± 1.0	ns	16.1 ± 7.6	<0.005
C20	1.8 ± 0.4	ns	3.1 ± 0.6	<0.001
C22	1.9 ± 0.9	ns	1.6 ± 0.4	<0.05
C24	1.2 ± 0.1	ns	1.6 ± 0.0	<0.005
C24:1	1.6 ± 0.9	ns	2.0 ± 0.4	<0.05
Cortex				
C16	2.6 ± 0.9	<0.01	13.1 ± 3.7	<0.005
C18	4.3 ± 2.1	<0.01	11.2 ± 2.3	<0.005
C18:1	1.3 ± 0.2	ns	21 ± 9.6	<0.01
C20	2.8 ± 1.1	ns	5.3 ± 0.7	<0.001
C22	0.9 ± 0.2	ns	2.6 ± 0.4	<0.001
C24	1.1 ± 0.2	ns	2.3 ± 0.4	<0.01
C24:1	2.4 ± 1.0	ns	3.3 ± 0.8	<0.01
VPM/VPL				
C16	1.6 ± 0.3	<0.05	10.0 ± 2.5	<0.001
C18	2.8 ± 0.8	<0.05	23.9 ± 7.6	<0.001
C18:1	0.3 ± 0.1	ns	9.8 ± 3.7	<0.001
C20	1.1 ± 0.4	ns	7.3 ± 2.0	<0.005
C22	1.0 ± 0.2	ns	3.5 ± 1.2	<0.010
C24	3.2 ± 1.1	ns	2.1 ± 0.6	<0.010
C24:1	1.1 ± 0.2	ns	1.4 ± 0.2	n.s
PAG				
C16	2.2 ± 0.5	<0.05	4.7 ± 2.9	<0.05
C18	2.0 ± 0.4	<0.001	6.7 ± 2.4	<0.05
C18:1	5.9 ± 2.5	<0.05	4.7 ± 3.0	ns
C20	3.4 ± 2.0	ns	3.9 ± 1.1	<0.05
C22	3.6 ± 0.8	ns	1.6 ± 0.3	ns
C24	4.8 ± 2.6	<0.05	1.3 ± 0.3	ns
C24:1	6.2 ± 2.7	ns	1.3 ± 0.4	ns

Values are means ± s.e.m. $n = 4–5$. ns = not significant.

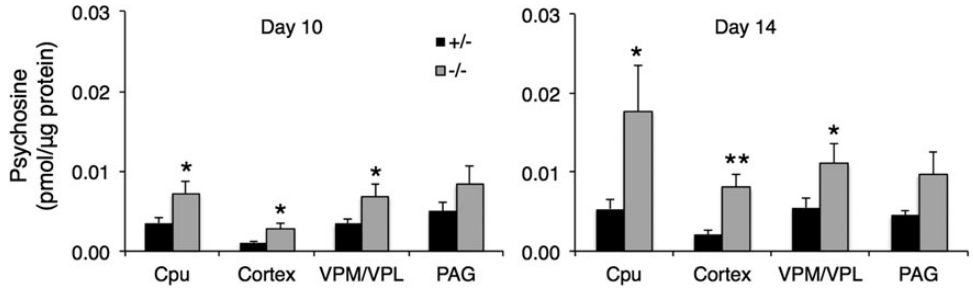

Figure 3. Psychosine levels in nGD brains at 10 and 14 days. Values are means ± s.e.m., $n = 4–5$. $^{*}P < 0.05$, $^{**}P < 0.01$.

Table 2. Fold-change of psychosine in different brain areas at different ages

10-day-old mice Ratio (−/− versus +/−)	*P*-value	14-day-old mice Ratio (−/− versus +/−)	*P*-value
CPu			
2.1 ± 0.5	ns	3.7 ± 1.0	<0.05
Cortex			
2.6 ± 0.5	<0.05	7.1 ± 3.1	<0.01
VPM/VPL			
2.8 ± 1.0	ns	2.5 ± 0.7	<0.05
PAG			
1.5 ± 0.3	ns	2.0 ± 0.4	ns

Values are means ± s.e.m. $n = 4–5$. ns = not significant.

age (Fig. 6). Together, the LC-ESI-MS/MS data indicate that a certain level of GlcCer accumulation, but not of psychosine, is required to trigger neuropathological changes in specific brain areas, while other brain areas containing similar GlcCer levels are unaffected.

Ultrastructural evaluation of GlcCer storage in the nGD brain

To investigate the cellular and subcellular localization of GlcCer accumulation, we examined the cerebral cortex and VPM/VPL of 14, 18 and 21-day-old −/− mice by transmission electron microscopy. GlcCer accumulation (31,32) was readily apparent in cortical neurons from 14-day-old mice (Fig. 7). Fibrils and characteristic 'pseudotubular' structures, also referred to as 'twisted tubules' and attributed to GlcCer accumulation (31,32), were frequently found in the cell body of large neurons (Fig. 7A–F), but were never observed in control mice. When viewed in transverse (Fig. 7C), the diameter of individual pseudotubules was 300–400 Å, consistent with the reported size for GlcCer storage tubules (3,31). The inclusions often resided near the nucleus (Fig. 7A–F) without a particular orientation, but also extended into the base of dendrites (Fig. 7G). The storage material was present in a membrane-delimited, vacuolar compartment and varied in density from sparse (Fig. 7A–D) to dense (Fig. 7E and F). Few, if any, pseudotubules were found in the cytoplasm (Fig. 7G). nGD cortical neurons, with or without pseudotubules, displayed some distension of endoplasmic reticulum (ER) cisternae (Fig. 8). Other cytoplasmic inclusions were occasionally present in nGD neurons (e.g. Fig. 7B) but these were not definitively more abundant than in control neurons.

A more severely affected cellular phenotype, displaying highly extensive cytoplasmic inclusions, was observed in the cortex and thalamus, particularly of 18 and 21-day-old mice (Figs 9 and 10). These cells did not appear to be astrocytes, oligodendrocytes or microglia since they did not display fibrillar intermediate filaments or conspicuous glycogen granules typical of astrocytes (33), dark or heterochromatic nuclei or electron-dark cytoplasm typical of oligodendrocytes or microglia (33), or a dilated nuclear envelope typical of oligodendrocytes (33). While not as immediately identifiable, these cells were most-likely neurons displaying a distinct morphology resulting from advanced pathology. Large accumulations of densely packed pseudotubules were observed in these cells (Figs 9 and 10), sometimes as one inclusion body that reached a size as large as the nucleus (Fig. 9G) and that displayed an irregular, curvilinear contour (Figs 9A and G, and 10A and D). Inclusions contained pseudotubules at varied orientations, resulting in round, oblong and rod-like shapes (Fig. 9D and F) upon sectioning, and ranged from ∼250 to 400 Å in diameter. Long, thin meandering membrane-bound extensions arose from, and often appeared to link separate pseudotubular inclusions (Figs 9D and E, and 10A). Furthermore, some extensions were continuous with the plasma membrane, suggesting the inclusions were accessible to the extracellular space (Figs 9B and 10A).

In addition to the significant degree of GlcCer storage, these neurons showed additional pathology with signs of degeneration. The cytoplasm revealed many varied electron-dense inclusions and lighter vacuolar bodies (Figs 9A, D and F, and 10A and D). In most cases, these structures, together with pseudotubules, formed a large, pleiomorphic, membrane-delimited body (Fig. 10A and D). Autophagosomes were also abundant (Fig. 10) and were observed to fuse with the larger pleiomorphic masses (Fig. 10B). Not uncommon for normal neurons, long and/or parallel cisternae of ER were often present (Figs 9A, C and G and 10A), but appeared unusually narrow (e.g. Fig. 9C). Nuclei were located eccentrically in the cell body and were oval, bean-shaped or indented rather than round. Nucleoli characteristic of neurons were present, though located eccentrically in the nucleus, and the karyoplasm was heterochromatic, with condensed chromatin lining the nuclear envelope (Figs 9A and G and 10A inset, D). Some neurons displayed more than one nuclear profile (Fig. 10D), though it is possible that these were components of an indented nucleus disrupted in shape by the large inclusions. Multiple, relatively narrow cytoplasmic extensions arose from the cell body, sometimes branching immediately (Figs 9C and 10D). The autophagic activity, abnormal nuclear

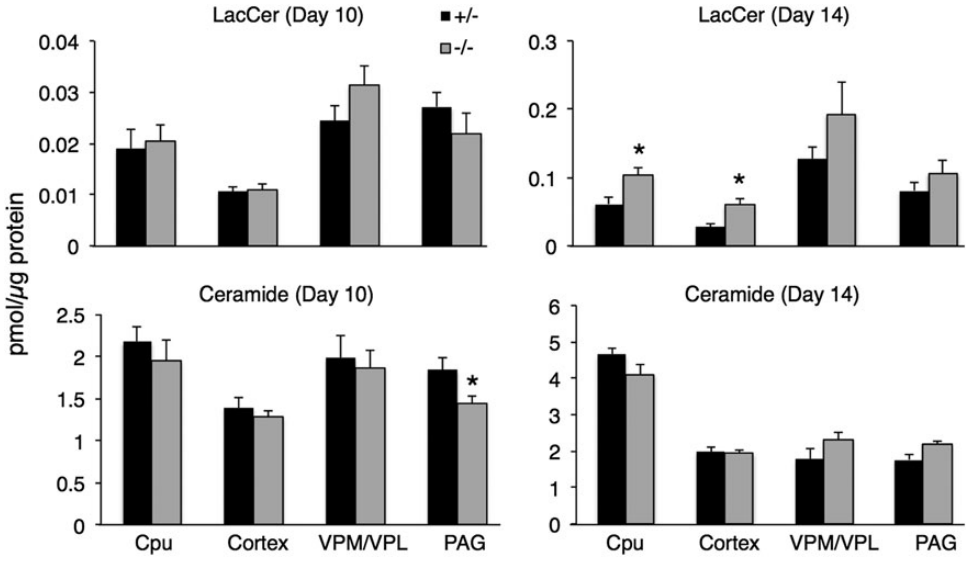

Figure 4. Lactosylceramide and ceramide levels in nGD brains at 10 and 14 days. Values are means ± s.e.m., $n = 4–5$.*$P < 0.05$.

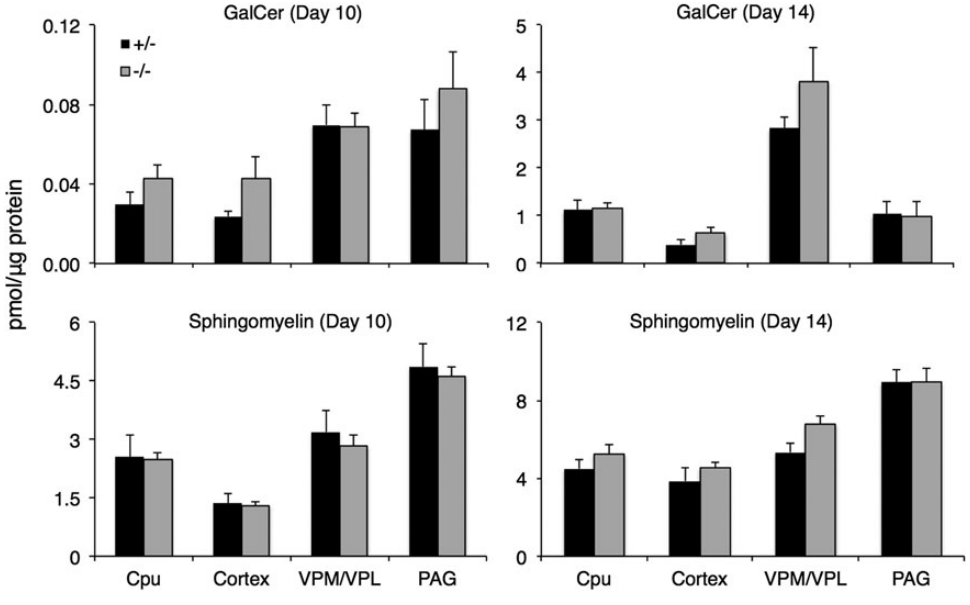

Figure 5. Galactosylceramide and sphingomyelin levels in nGD brains at 10 and 14 days. Values are means ± s.e.m., $n = 4–5$.

findings and atypical cytoplasmic extensions suggest that these heavily storage-laden neurons may have been in the process of undergoing cell death.

DISCUSSION

In the current study, we delineate the relationship between SL accumulation and the development of brain pathology in nGD, by providing LC-ESI-MS/MS data on the SL content of specific brain areas that display different degrees of pathology, and by ultrastructural examination of GlcCer storage and associated cytopathology. Since data obtained from human patients is naturally limited to post-mortem tissue from end-stage disease (10,11,18), the use of mouse models provides an important tool for analyzing changes in the lipid and ultrastructural profiles in pre-symptomatic stages, and in particular, for comparing these changes with other pathological processes such as neuron loss and neuroinflammation. The nGD mouse model that was used in the current study was the $Gba^{flox/flox}$;nestin-Cre mouse, in which GCase deficiency is restricted to neurons and macroglia, with normal GCase activity in microglia (20,34). This model was used since a complete GCase knock-out mouse dies hours after birth due to skin permeability defects (reviewed in 34), and disease progression in a mouse in which GCase activity is restored in skin tissue is extremely rapid (20,34), rendering it difficult to distinguish the different disease stages.

Prior to mass spectrometry and ultrastructural analyses, a set of experiments was performed to analyze GlcCer accumulation

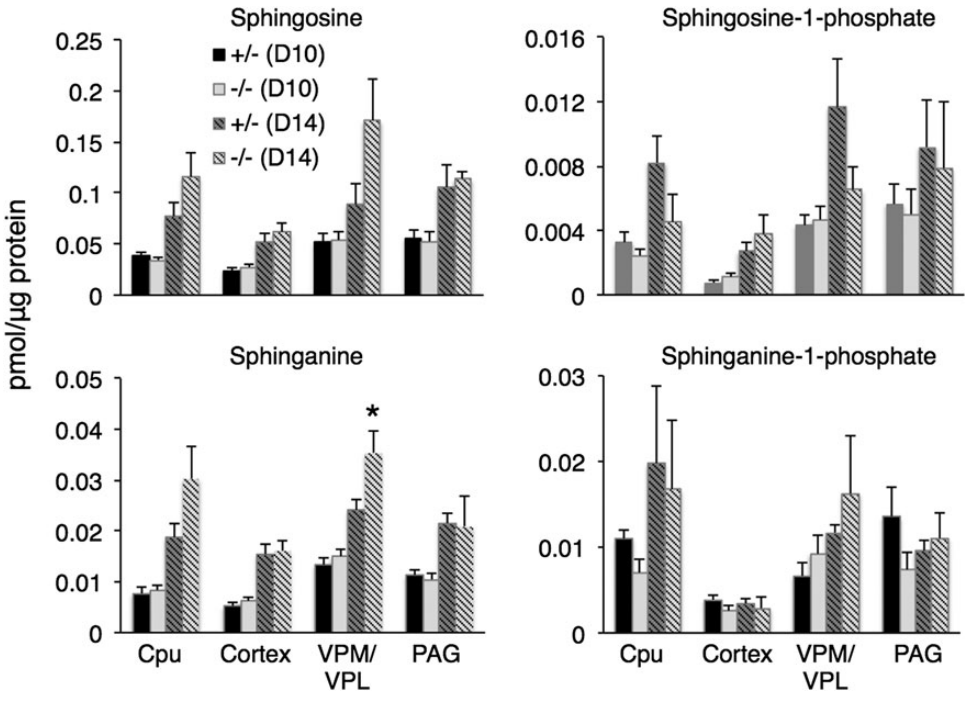

Figure 6. Levels of long chain bases in nGD brains at 10 and 14 days. $n = 4–5 \pm$ s.e.m. Values are means $\pm$ s.e.m., $n = 4–5$. $^{*}P < 0.05$.

in situ using the Periodic acid-Schiff (PAS) stain, which labels tissue carbohydrates (35) and has been widely used to label 'Gaucher cells' (i.e. peripheral macrophages which store large quantities of GlcCer) (36). PAS staining in the −/− brain was evident in all brain areas that exhibited neuroinflammation and neuron loss (19), and in many cases appeared in cells that displayed neuronal morphology. However, closer examination suggested that PAS might be labeling degenerating neurons irrespective of whether these cells accumulated GSLs (37), possibly due to changes in carbohydrate metabolism upon neuronal degeneration (38). Thus, although PAS staining can be used to detect GlcCer accumulation in viable Gaucher tissues, its use in the CNS may be problematic. Direct visualization of GlcCer accumulation in nGD brains awaits the availability of suitable tools, such as reliable anti-GlcCer antibodies or *in situ* mass spectrometry techniques.

Although previous studies have used mass spectrometry to examine SL levels in Gaucher brain, they did not distinguish between brain areas that did or did not display pathology, but rather measured global changes in brain SLs (14,39). In contrast, we analyzed SL levels in specific brain areas that displayed selective vulnerability, and at specific time-points of disease progression. As previously reported (for example 10,11), we demonstrate that GlcCer and psychosine specifically accumulate in nGD brain, and that LacCer levels are slightly elevated (10). However, there was no correlation between levels of ceramide (40), sphingoid long chain bases or psychosine, and neuronal loss. Loss of GCase activity did not lead to a reduction in ceramide levels, suggesting that GCase does not significantly contribute to cellular ceramide levels, at least in nGD. Moreover, ceramide levels are unlikely to be altered in GD carriers, rendering it highly unlikely that changes in cellular ceramide levels contribute to the mechanistic connection between GD and Parkinson's disease (29,30).

The mass spectrometry data are consistent with a model, whereby GlcCer accumulates to a similar extent in most brain areas, and the reason for selective vulnerability is largely due to intrinsic differences in the neurons in different brain areas, or due to differences in the neuronal environment. Although psychosine accumulates in nGD brain tissues at a pre-symptomatic stage, there was no correlation between its levels and the appearance of neuropathology, which was somewhat surprising since psychosine has been implicated as the offending lipid in nGD, accumulates significantly in human and mouse brain (10,14), and appeared to correlate with the degree of severity of nGD signs in human patients (10,15). Addition of psychosine to a cultured cholinergic neuron-like cell line, LA-N-2, led to cell death (16), but the levels used (1–10 µM) were significantly higher than those reported in the nGD human brain (41). The fact that psychosine levels are ∼140-fold lower than GlcCer levels, and that psychosine levels do not progressively accumulate at the critical time of disease initiation in the nGD mouse, strongly suggest that it is not the causative pathological agent.

Other studies reported a greater fold-elevation in psychosine (13–15) levels. However, the absolute levels of psychosine in our study compare favorably with other published data. For instance, the first measurement of psychosine in human post-mortem Gaucher brain gave values in the range of 0.05 nmol/mg protein, similar to our values. Other studies in human and mouse brain gave values about 50-fold higher. It should be noted that our data was obtained from pre-symptomatic brain tissues from a mouse model in which only a subset of brain cells (i.e. those from a neuronal lineage) were depleted of GCase, in which psychosine levels are likely to be lower than in mouse models completely deficient in GCase or from human tissues obtained post-mortem.

In addition to the quantitative measurements performed by LC-ESI-MS/MS, we analyzed GlcCer accumulation by electron

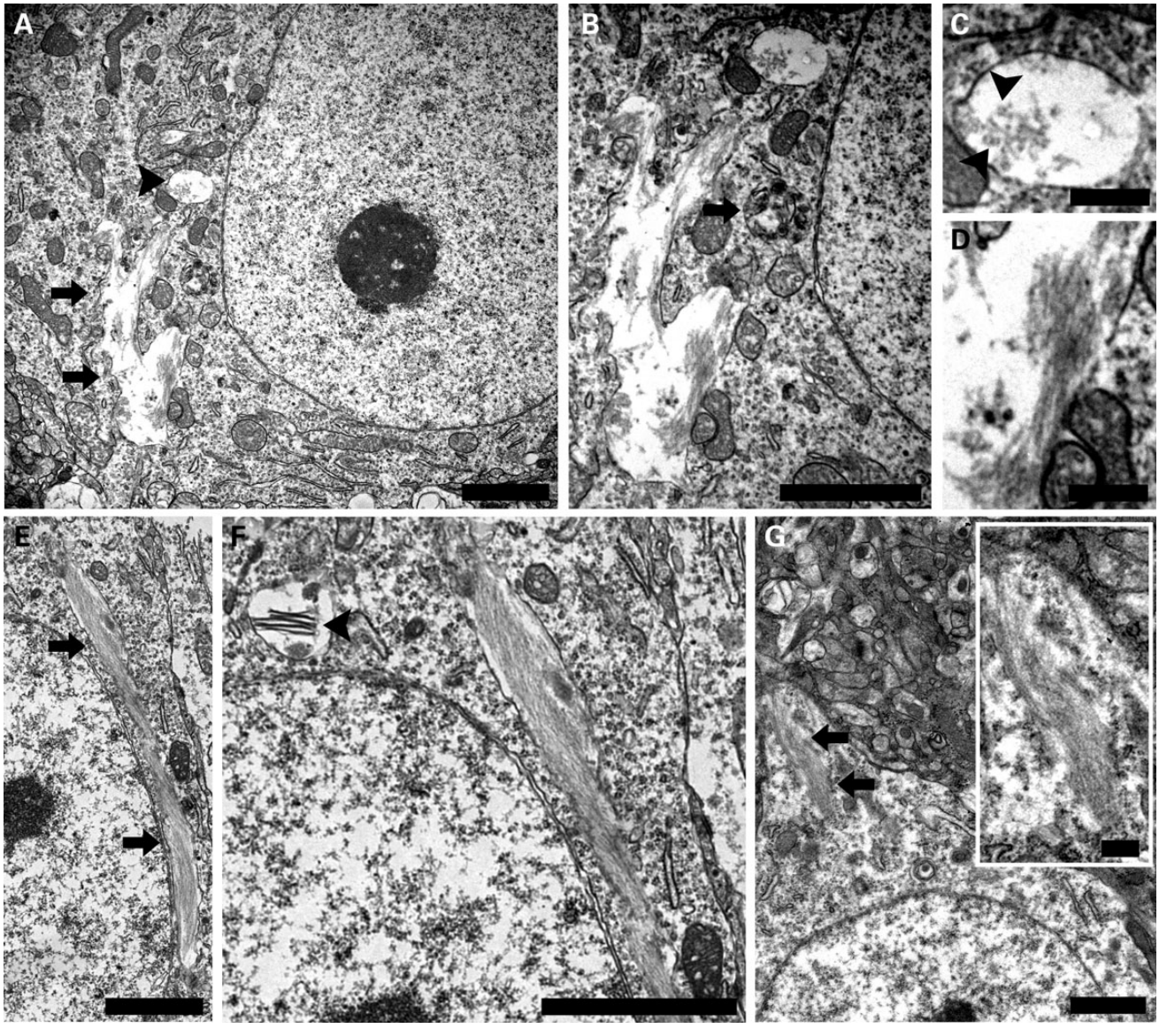

Figure 7. Ultrastructure of GlcCer storage in nGD neurons. Neurons were from the cerebral cortex of −/− mice at 14 (**A**–**F**) and 21 (**G**) days of age. (A–D) A prominent vacuolar inclusion (arrows in A) in the perikaryoplasm of a large neuron to the left of the nucleus, containing dilute arrays of fibrils and pseudotubules, most of which are longitudinal but sometimes transverse as in the upper vacuole (arrowhead in A), which is probably a continuation of the same membrane-bound compartment indicated by the arrows. (B–D) Higher magnifications of the inclusions so as to resolve the encompassing membrane and the tubular appearance of its contents (C and D) seen in cross-section in (C) (arrowheads). An unrelated inclusion body (arrow) is also present in (B). (**E** and **F**) A large neuron with an inclusion body (arrows) (∼9 μm in length) showing more densely packed pseudotubules. A rounded vacuole in (F) includes dense fibrils (arrowhead) that might correspond to flattened GlcCer bilayer stacks (32). (**G**) A neuron with pseudotubules (arrows) running into a process which is not clearly membrane-delimited (further magnified in the inset). Scale bars are all 2 μm except for (**C**) and (**D**) which are 0.5 μm.

microscopy, and observed significant accumulation in neurons. Fibrils and pseudotubules were of the expected diameter and were similar to those previously observed (11,12,17,23,31,32,42,43). The tubules are formed by a series of parallel membrane-like bilayers composed of GlcCer, and are twisted longitudinally, giving the impression of tubular structures (32). To our knowledge, such structures have not been found in other lysosomal storage disorders. The existence of such structures within neurons has been debated, and when shown, were relatively rare (11,12,17,18,23,42). In the current study, we detected common neuronal inclusions in the cerebral cortex; however, the neuronal inclusions were not always large or electron dense, making it relatively easy to miss them.

In peripheral Gaucher cells, pseudotubules are found as membrane-bound inclusions, although discontinuities in the limiting membrane have been reported (43). Non-membrane bound cytosolic fibrils and pseudotubules have been reported in neurons (42) and in perivascular cells in human CNS tissue (44), but it has also been suggested that these were misidentified cytoskeletal elements (11). We now show that pseudotubules in neurons are contained within a membrane-bound compartment, with only rare evidence of unbound material in the cytosol. The

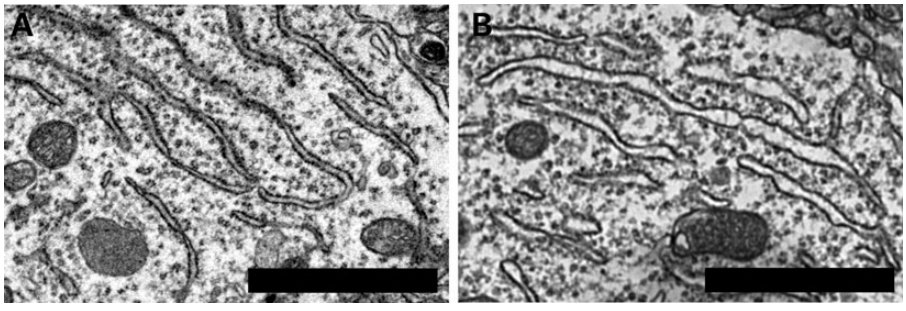

Figure 8. Distention of ER cisternae in nGD neurons. Sample arrays of rough ER in cerebral cortex neurons of (**A**) +/− and (**B**) −/− mice at 14 days of age. Scale bars are 2 μm.

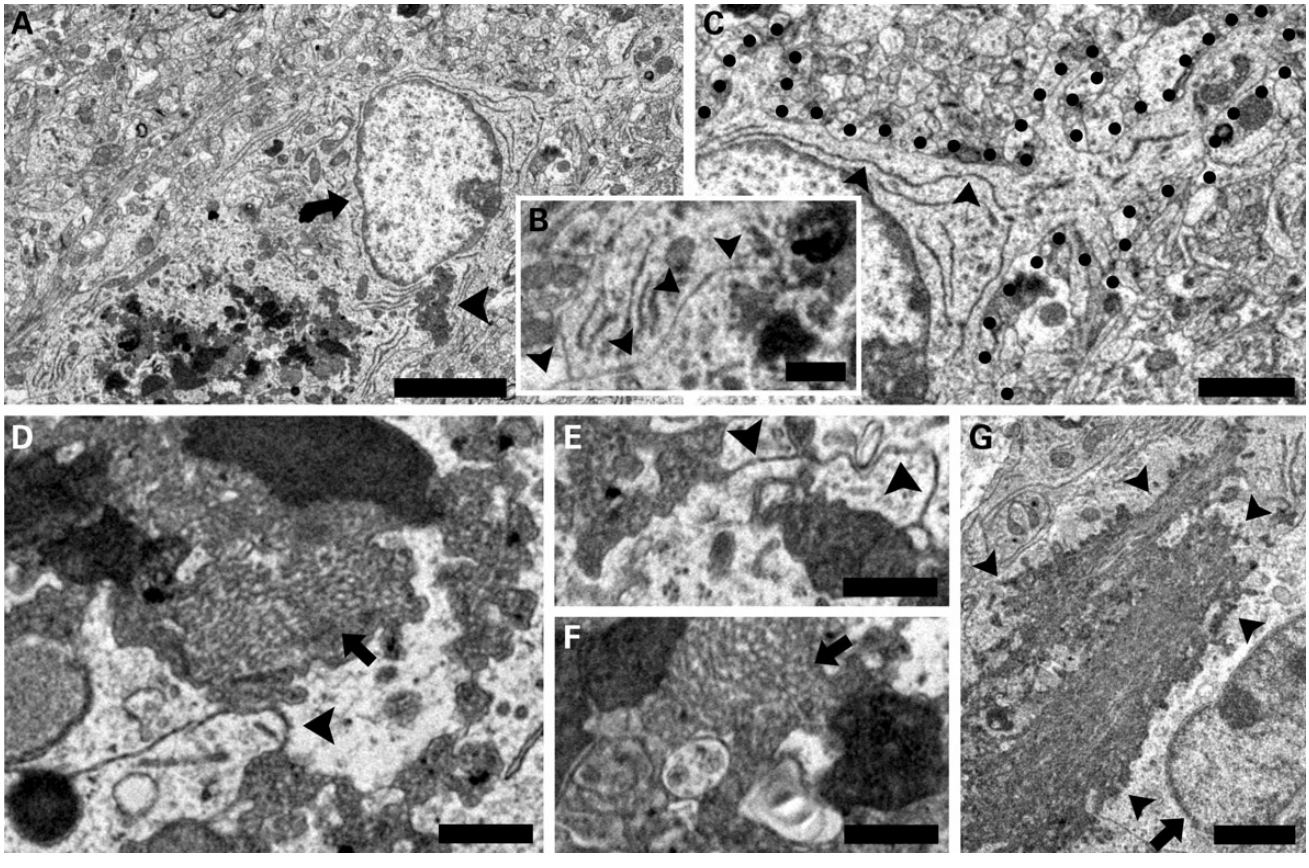

Figure 9. Neurons showing progression of storage and additional pathology**.** Samples were from the cerebral cortex of nGD mice at 18 days of age (**A**–**F**) and from the VPM/VPL at 21 days of age (**G**). (A) A cell with a modestly heterochromatic nucleus (arrow) and an eccentric nucleolus showing numerous pseudotubular inclusions (arrowhead), or amassed with other inclusions (lower left-half). (B) A magnification of the lower-left corner of (A) shows some inclusions that are continuous (arrowhead sequence) with the plasma membrane and extracellular space (electron-lucent area in lower left). (C) A magnification of the upper right region of the cell shown in (A) shows cytoplasmic extensions (dots mark the cell perimeter). Note the presence of long, relatively-narrow ER cisternae (indicated by arrowheads). (D–F) Enlargement of portions from the lower part of the cell shown in (A) shows morphologically diverse constituents (D and F), separate inclusion bodies tethered together through narrow extensions (arrowheads in D and E), and bodies containing densely packed arrays of pseudotubules at various orientations (arrows in D and F). (G) A cell with a somewhat heterochromatic nucleus (arrow) and huge inclusion (arrowheads) of up to ∼12 μm in length, containing densely packed pseudotubules, many of which are oriented longitudinally. Scale bars: (A) 4 μm; (B) 1 μm; (C and G) 2 μm; (D–F) 0.5 μm.

dominant view for the identity of the vacuolar compartment in Gaucher cells is the lysosome (23,43), although evidence has been obtained that GlcCer can also accumulate in the ER (11,41,42,45); however, the extent of ER accumulation was not sufficient to activate the unfolded protein response (UPR), at least in neuronal models of nGD (46). We now find further evidence that neurons from nGD mice display dilations of ER cisternae (11,42) at early stages of storage. Further studies, using specific immunohistochemical markers together with quantitative imaging approaches, will be required to clarify the involvement of the ER in the development of nGD pathology.

We also document a more severe neuronal phenotype, which was more prominent in the latter stages of the disease. These neurons displayed huge pseudotubular structures of the expected

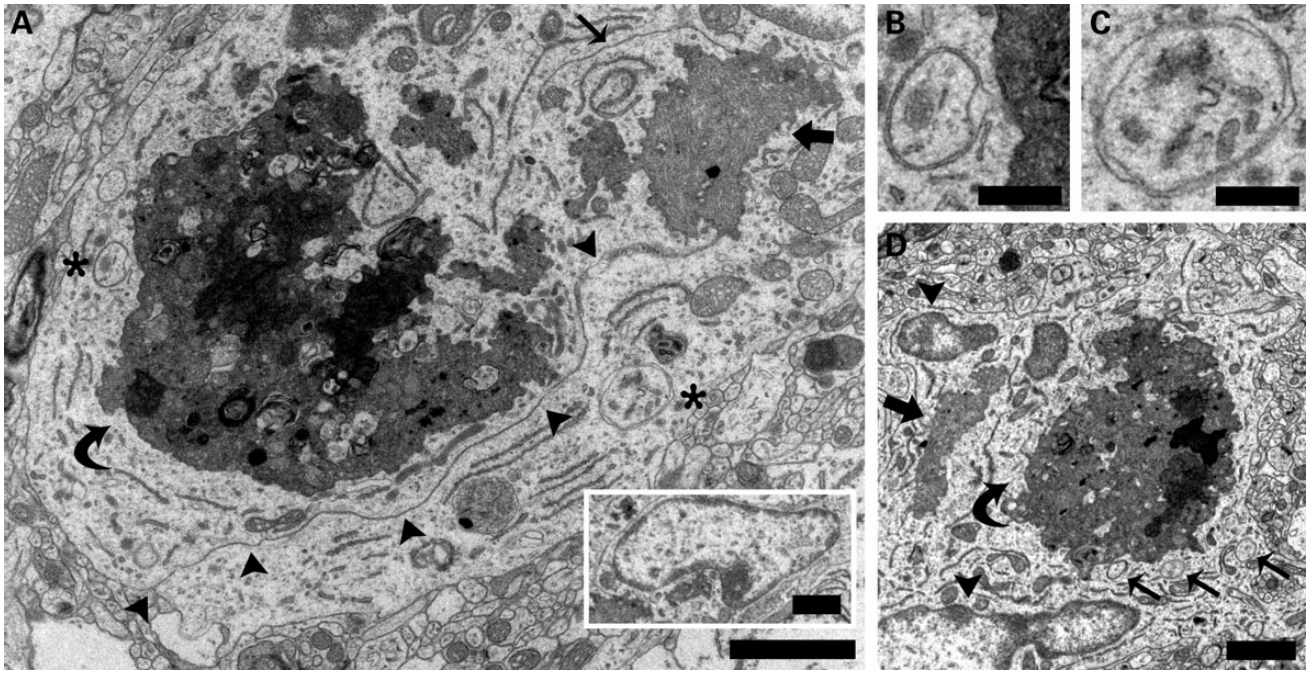

Figure 10. Additional ultrastructural features of highly disrupted neurons**.** Samples were from the cerebral cortex of nGD mice at 18 days of age. (**A**) A cell with a large mass of pseudotubules (arrow) and one very large (∼7 μm) membrane-bound, pleiomorphic inclusion (curved arrow). The cell nucleus, cut off at the upper right, is shown fully in the inset. The large, independent pseudotubule mass shows an extension (thin arrow) leading to another small inclusion. The path of another longer extension suggests continuity with the plasma membrane and extracellular space (arrowheads). The cell has several autophagosomes (on the right of the asterisks). (**B** and **C**) Magnifications of two autophagosomes from the cell shown in (A), with both showing a double membrane and one (B) in the process of fusing with the pleiomorphic body on its right. (**D**) This cell also shows a large pseudotubule-containing body (arrow), a pleiomorphic membrane-bounded mass (curved arrow) (up to 8 μm), several short cytoplasmic extensions (upper and lower right) and numerous autophagosomes (thin arrows). The cell displays two heterochromatic nuclear profiles (arrowheads). Scale bars: (A), (A) inset, (D) 2 μm; (B and C) 0.5 μm.

size for GlcCer deposits (31,43), but were more compact than those found in neurons that displayed more modest storage, and resembled pseudotubular structures from peripheral Gaucher cells (17,32) and macrophages (12,23). When caught at transverse angles, collections of pseudotubules also resembled cross-sections of GlcCer deposits isolated from human spleen Gaucher cells (32). Interestingly, the irregular profile of these inclusions, and the pattern of interconnectivity between them, resembles that previously observed in diseased microglia (23). Although it might be argued that the severely affected cells that we observe are microglia that phagocytosed dead neurons, we consider this unlikely since their overall ultrastructure did not match that of microglia (33). Moreover, the persistence of very large pseudotubular inclusions independent of putatively phagocytosed material is inconsistent with the fact that microglia in the mouse model employed in the current study express normal GCase activity (20).

Overall, the ultrastructural observations suggest that neurons accumulate GlcCer fibrils and pseudotubules in vacuolar compartments and then continue to further develop larger, denser masses of pseudotubules. The additional varied inclusions, often seen as one pleiomorphic body, might be due to a more generalized disturbance in lysosomal function (47). Indeed, a recent study suggested that the autophagic machinery is defective in cultured neurons lacking GCase (48). The frequent presence of numerous autophagosomes, which were also seen to fuse with the pleiomorphic inclusions, supports the idea that this large body may be forming as part of the course of cell death. The presence of numerous small cytoplasmic extensions, nuclei which are relatively heterochromatic for neurons and situated eccentrically in the perikaryoplasm, and evidence of more than one nuclear profile, lend additional support to the view that these are degenerating neurons. Similar to the dense pseudotubule-containing compartments continuous with the plasma membrane, rare evidence of large inclusions situated near the plasma membrane have been reported in human peripheral Gaucher cells (43). We contend that the long continuities in neurons, together with the cytoplasmic extensions, are likely to represent the beginning of cytoplasmic fragmentation as an early event of cell death. In summary, the EM findings suggest that neuronal GlcCer storage may be more significant than previously thought. Moreover, pending definitive identification and further evaluation of degenerative changes, the ultrastructural studies imply that intrinsic storage is a major determinant of neuronal cell demise.

Together, the current study is consistent with a model, whereby GlcCer accumulates to a similar extent in most brain areas, and upon reaching a certain threshold of accumulation, a series of secondary events is triggered which includes neuroinflammation and neurodegeneration (19,21) that subsequently cause neuronal death (19). However, this cascade is only triggered in specific brain areas, which reflects their sensitivity to GlcCer accumulation, presumably due to an intrinsic property of the neurons in that brain area. Within an affected brain area, neuronal GlcCer storage appears to be a substantial contributor to neurodegeneration. Understanding the basis for this selective

sensitivity and the precise biochemical pathways triggered in neurons by GlcCer storage will be in the focus of further studies.

MATERIALS AND METHODS

Mice

$Gba^{flox/flox}$; nestin-Cre mice were used as a model of nGD, in which GCase deficiency is restricted to neurons and macroglia with normal GCase activity in microglia (20). $Gba^{flox/flox}$ mice were crossed with $Gba^{flox/wt}$; nestin-Cre mice to generate $Gba^{flox/flox}$; nestin-Cre mice (referred to as −/− mice) and $Gba^{flox/wt}$; nestin-Cre mice (referred to as +/− mice), which served as healthy controls since they do not show any overt pathology (19). Genotyping was performed by polymerase chain reaction using genomic DNA extracted from mouse tails (46). Mice were maintained under specific pathogen-free conditions and handled according to protocols approved by the Weizmann Institute Animal Care Committee according to international guidelines.

Immunohistochemistry

Mac2 immunohistochemical staining was performed as described previously (19), using a rat anti-Mac2 antibody (1:1000, Cedarlane, Ontario, Canada).

Sample preparation for biochemical analysis

Ten and 14-day-old mice were sacrificed and their brains removed and placed on a Young Mouse Brain Slicer Matrix (BSMYS001-1, Zivic instruments, Pittsburgh, PA, USA). Single-edge razor blades were inserted into the matrix to generate 1 mm coronal sections. The sections containing the areas of interest were snap-frozen on dry ice, and a 17 g (1 mm diameter) blunt needle attached to a syringe was used to remove the CPu, VPM/VPL region of the thalamus, and the PAG. The cerebral cortex was separated using a spatula from the same section containing the VPM/VPL. Each brain area was placed in a microcentrifuge tube, snap-frozen in liquid N_2 and stored at −80°C. All dissection tools were first cleaned with surface decontaminant RNase Away (Molecular BioProducts, Inc., San Diego, CA, USA).

RNA extraction and quantitative polymerase chain reaction

Total RNA was isolated using the RNeasy mini kit (Qiagen GmbH, Hilden, Germany) according to manufacturer's instructions, which included DNase treatment and addition of β-mercaptoethanol. cDNA synthesis was performed using the Reverse-iT first-strand synthesis kit (Thermo Fisher Scientific, Surrey, UK) using random decamers. cDNA products were stored at −20°C. Quantitative polymerase chain reaction (PCR) was performed using PerfeCTa SYBR Green FastMix (Quanta BioSciences, Gaithersburg, MD, USA) and an ABI Prism 7300 Sequence Detection System (Applied Biosystems, Foster City, CA, USA). The primer concentration was 13 nM in a reaction volume of 20 μl and cDNA equivalent to 2–20 ng of total RNA. Each reaction was performed in triplicate. The thermal cycling parameters were as follows: step 1, 95°C for 10 min; step 2, 95°C for 15 s, 60°C for 30 s and 68°C for 30 s. Step 2 was repeated for 40 cycles and was followed by a dissociation step. Fold-change in mRNA levels was calculated using the comparative cycle threshold method using TATA box binding protein (TBP) for normalization. *P*-values were calculated using a two-tailed, two-independent sample Student's *t*-test. Primers sequences were as follows:

TBP: forward: 5′-TGCTGTTGGTGATTGTTGGT-3′; Reverse: 5′-CTGGCTTGTGTGGGAAAGAT-3′; Mac2 (LGALS3): Forward: 5′-CACTGACGGTGCCCTATGAC-3′; Reverse: 5′-AACAATCCTGTTTGCGTTGGG-3′.

GCase activity assay

Frozen brain samples were sonicated in McIlvaine's buffer (0.1 M citric acid, pH 4.2, 0.2 M Na_2HPO_0, 29:21, vol:vol) and protein concentration estimated by the BCA protein assay reagent (Pierce Chemical Co., Thermo Scientific, Rockford, IL, USA). Tissue homogenates containing 25 or 50 μg of protein were incubated at 37°C with 8 μM C6-NBD-GlcCer (Avanti Polar Lipids, Alabaster, AL, USA) in a final volume of 50 μl McIlvaine's buffer (49) for 3 or 1 h, respectively (50). Reactions were terminated by addition of three volumes of chloroform:methanol (1:2, vol:vol). Lipids were extracted (51) and the lower phase separated by thin layer chromatography using chloroform:methanol:9.8 mM $CaCl_2$ (60:35:8, vol:vol:vol) as the developing solvent. C6-NBD-ceramide was identified with an authentic standard using a Typhoon 9410 variable mode imager and bands were quantified by Image-QuantTL (GE Healthcare, Chalfont St Giles, UK).

Sphingolipid analysis

LC-ESI-MS/MS was performed using an ABI 4000 quadrupole-linear ion trap mass spectrometer (52,53) using sphingolipid internal standards from Avanti Polar Lipids (Alabaster, AL, USA). The standard used to reference the MS data for the quantitation of psychosine was a chemically defined glucosyl (ß) sphingosine (d18:1). *P*-values were calculated using a one-tailed or two-tailed, two-independent sample Student's *t* test.

Transmission electron microscopy

Mice were anesthetized and perfused transcardially with 2% paraformaldehyde, 1.5% glutaraldehyde in 0.1 M cacodylate buffer, pH 7.4. Brains were dissected and post-fixed in the same solution for 24 h at 4°C and then embedded in 7% agarose and sectioned (200 μm) using a vibratome (Electron Microscopy Sciences, Hatfield, PA, USA). Sections were incubated in 1% osmium tetroxide in 0.1 M cacodylate (1 h), stained with 2% uranyl acetate in water (1 h) and dehydrated in graded ethanol solutions. A 17 g blunt needle was used to remove the VPM/VPL; the cerebral cortex was separated from the same brain section and the tissues were embedded in Epon 812 (Electron Microscopy Sciences, Fort Washington, PA, USA). 70–90 nm sections were cut using an ultramicrotome (UCT, Leica, Wetzlar, Germany). Sections were examined using a SPIRIT Transmission Electron Microscope (FEI, Eidhoven, Netherlands) and digitized with an EAGLE CCD camera using TIA software (FEI, Eidhoven, Netherlands), or with a Phillips CM10 transmission electron microscope equipped with a Morada 14-bit digital

camera and iTEM software (Olympus Soft Imaging Solutions) for direct image acquisition. The sections that were examined were from the cortex of 14-day-old nGD mice ($n = 2$), cortex and VPM/VPL from 18-day-old nGD mice ($n = 1$), cortex from 21-day-old nGD mice ($n = 2$) and control ($+/-$) mice from the same ages. Images were prepared using Adobe Photoshop CS2 software to convert data to 8-bit, and to adjust brightness and contrast (with gamma factor fixed to 1) to achieve suitable visibility of ultrastructural details.

ACKNOWLEDGMENTS

We thank Dr Stefan Karlsson for originally providing the $Gba^{flox/flox}$;nestin-Cre nGD mice, Dr Smadar Zaidman from the Weizmann Institute Electron Microscopy Unit and Ran Salomon for electron microscopy sample preparation. A.H.F. is the Joseph Meyerhoff Professor of Biochemistry at the Weizmann Institute of Science.

Conflict of Interest statement. None declared.

FUNDING

The electron microscopy analyses conducted in the Cell and Molecular Neuroimaging Core facility at the Albert Einstein College of Medicine of Yeshiva University was supported by an NIH/NICHD Center grant (#P30HD071593) for Research on Intellectual and Developmental Disabilities. This work was generously supported by the Children's Gaucher Research Fund.

REFERENCES

1. Farfel-Becker, T. and Futerman, A.H. (2010) Cellular pathogenesis in sphingolipid storage disorders: the quest for new therapeutic approaches. *Clin. Lipidol.*, **5**, 255–265.
2. Vitner, E.B., Platt, F.M. and Futerman, A.H. (2010) Common and uncommon pathogenic cascades in lysosomal storage diseases. *J. Biol. Chem.*, **285**, 20423–20427.
3. Beutler, E. and Grabowski, G.A. (2001) Gaucher Disease. In Scriver, C., Beaudet, A.L., Valle, D., Sly, W.S. and Childs, B. (eds), *The Metabolic and Molecular Bases of Inherited Disease*. McGraw-Hill, New-York, Vol. 3, pp. 3635–3668.
4. Mignot, C., Doummar, D., Maire, I. and De Villemeur, T.B., French Type 2 Gaucher Disease Study Group. (2006) Type 2 Gaucher disease: 15 new cases and review of the literature. *Brain Dev.*, **28**, 39–48.
5. Gupta, N., Oppenheim, I.M., Kauvar, E.F., Tayebi, N. and Sidransky, E. (2011) Type 2 Gaucher disease: phenotypic variation and genotypic heterogeneity. *Blood Cells Mol. Dis.*, **46**, 75–84.
6. Harris, C.M., Taylor, D.S. and Vellodi, A. (1999) Ocular motor abnormalities in Gaucher disease. *Neuropediatrics*, **30**, 289–293.
7. Sidransky, E., Nalls, M.A., Aasly, J.O., Aharon-Peretz, J., Annesi, G., Barbosa, E.R., Bar-Shira, A., Berg, D., Bras, J., Brice, A. *et al.* (2009) Multicenter analysis of glucocerebrosidase mutations in Parkinson's disease. *N. Engl. J. Med.*, **361**, 1651–1661.
8. Altarescu, G., Hill, S., Wiggs, E., Jeffries, N., Kreps, C., Parker, C.C., Brady, R.O., Barton, N.W. and Schiffmann, R. (2001) The efficacy of enzyme replacement therapy in patients with chronic neuronopathic Gaucher's disease. *J. Pediatr.*, **138**, 539–547.
9. Jmoudiak, M. and Futerman, A.H. (2005) Gaucher disease: pathological mechanisms and modern management. *Br. J. Haematol.*, **129**, 178–188.
10. Nilsson, O. and Svennerholm, L. (1982) Accumulation of glucosylceramide and glucosylsphingosine (psychosine) in cerebrum and cerebellum in infantile and juvenile Gaucher disease. *J. Neurochem.*, **39**, 709–718.
11. Conradi, N.G., Sourander, P., Nilsson, O., Svennerholm, L. and Erikson, A. (1984) Neuropathology of the Norrbottnian type of Gaucher disease. Morphological and biochemical studies. *Acta. Neuropathol.*, **65**, 99–109.
12. Tybulewicz, V.L., Tremblay, M.L., LaMarca, M.E., Willemsen, R., Stubblefield, B.K., Winfield, S., Zablocka, B., Sidransky, E., Martin, B.M. and Huang, S.P. (1992) Animal model of Gaucher's disease from targeted disruption of the mouse glucocerebrosidase gene. *Nature*, **357**, 407–410.
13. Orvisky, E., Sidransky, E., McKinney, C.E., LaMarca, M.E., Samimi, R., Krasnewich, D., Martin, B.M. and Ginns, E.I. (2000) Glucosylsphingosine accumulation in mice and patients with type 2 Gaucher disease begins early in gestation. *Pediatr. Res.*, **48**, 233–237.
14. Cabrera-Salazar, M.A., DeRiso, M., Bercury, S.D., Li, L., Lydon, J.T., Weber, W., Pande, N., Cromwell, M.A., Copeland, D., Leonard, J. *et al.* (2012) Systemic delivery of a glucosylceramide synthase inhibitor reduces CNS substrates and increases lifespan in a mouse model of type 2 Gaucher disease. *PLoS One*, **7**, e43310.
15. Orvisky, E., Park, J.K., LaMarca, M.E., Ginns, E.I., Martin, B.M., Tayebi, N. and Sidransky, E. (2002) Glucosylsphingosine accumulation in tissues from patients with Gaucher disease: correlation with phenotype and genotype. *Mol. Genet. Metab.*, **76**, 262–270.
16. Schueler, U.H., Kolter, T., Kaneski, C.R., Blusztajn, J.K., Herkenham, M., Sandhoff, K. and Brady, R.O. (2003) Toxicity of glucosylsphingosine (glucopsychosine) to cultured neuronal cells: a model system for assessing neuronal damage in Gaucher disease type 2 and 3. *Neurobiol. Dis.*, **14**, 595–601.
17. Hernández, F. and Bueno, M. (1973) Infantile neurological Gaucher's disease in three siblings. An ultrastructural study. *Virchows Arch A Pathol. Pathol. Anat.*, **360**, 27–32.
18. Kaye, E.M., Ullman, M.D., Wilson, E.R. and Barranger, J.A. (1986) Type 2 and type 3 Gaucher disease: a morphological and biochemical study. *Ann. Neurol.*, **20**, 223–230.
19. Farfel-Becker, T., Vitner, E.B., Pressey, S.N.R., Eilam, R., Cooper, J.D. and Futerman, A.H. (2011) Spatial and temporal correlation between neuron loss and neuroinflammation in a mouse model of neuronopathic Gaucher disease. *Hum. Mol. Genet.*, **20**, 1375–1386.
20. Enquist, I.B., Lo Bianco, C., Ooka, A., Nilsson, E., Månsson, J.-E., Ehinger, M., Richter, J., Brady, R.O., Kirik, D. and Karlsson, S. (2007) Murine models of acute neuronopathic Gaucher disease. *Proc. Natl Acad. Sci. USA*, **104**, 17483–17488.
21. Vitner, E.B., Farfel-Becker, T., Eilam, R., Biton, I. and Futerman, A.H. (2012) Contribution of brain inflammation to neuronal cell death in neuronopathic forms of Gaucher's disease. *Brain*, **135**, 1724–1735.
22. Wong, K., Sidransky, E., Verma, A., Mixon, T., Sandberg, G.D., Wakefield, L.K., Morrison, A., Lwin, A., Colegial, C., Allman, J.M. *et al.* (2004) Neuropathology provides clues to the pathophysiology of Gaucher disease. *Mol. Genet. Metab.*, **82**, 192–207.
23. Willemsen, R., Tybulewicz, V., Sidransky, E., Eliason, W.K., Martin, B.M., LaMarca, M.E., Reuser, A.J., Tremblay, M., Westphal, H. and Mulligan, R.C. (1995) A biochemical and ultrastructural evaluation of the type 2 Gaucher mouse. *Mol. Chem. Neuropathol.*, **24**, 179–192.
24. Pewzner-Jung, Y., Ben-Dor, S. and Futerman, A.H. (2006) When do lasses (longevity assurance genes) become CerS (ceramide synthases)? Insights into the regulation of ceramide synthesis. *J. Biol. Chem.*, **281**, 25001–25005.
25. Merrill, A.H. (2011) Sphingolipid and glycosphingolipid metabolic pathways in the era of sphingolipidomics. *Chem. Rev.*, **111**, 6387–6422.
26. Laviad, E.L., Albee, L., Pankova-Kholmyansky, I., Epstein, S., Park, H., Merrill, A.H. and Futerman, A.H. (2008) Characterization of ceramide synthase 2: tissue distribution, substrate specificity, and inhibition by sphingosine 1-phosphate. *J. Biol. Chem.*, **283**, 5677–5684.
27. Ben-David, O. and Futerman, A.H. (2010) The role of the ceramide acyl chain length in neurodegeneration: involvement of ceramide synthases. *Neuromolecular Med.*, **12**, 341–350.
28. Sastry, P.S. (1985) Lipids of nervous tissue: composition and metabolism. *Prog. Lipid Res.*, **24**, 69–176.
29. Bras, J., Singleton, A., Cookson, M.R. and Hardy, J. (2008) Emerging pathways in genetic Parkinson's disease: potential role of ceramide metabolism in Lewy body disease. *FEBS J.*, **275**, 5767–5773.
30. Neumann, J., Bras, J., Deas, E., O'Sullivan, S.S., Parkkinen, L., Lachmann, R.H., Li, A., Holton, J., Guerreiro, R., Paudel, R. *et al.* (2009) Glucocerebrosidase mutations in clinical and pathologically proven Parkinson's disease. *Brain*, **132**, 1783–1794.
31. Lee, R.E. (1968) The fine structure of the cerebroside occurring in Gaucher's disease. *Proc. Natl Acad. Sci. USA*, **61**, 484–489.

32. Lee, R.E., Worthington, C.R. and Glew, R.H. (1973) The bilayer nature of deposits occurring in Gaucher's disease. *Arch. Biochem. Biophys.*, **159**, 259–266.
33. Peters, A., Palay, S.L. and Webster, H.D. (1991) *The Fine Structure of the Nervous System*. Oxford University Press, New York.
34. Farfel-Becker, T., Vitner, E.B. and Futerman, A.H. (2011) Animal models for Gaucher disease research. *Dis. Model Mech.*, **4**, 746–752.
35. Wolman, M. (1950) Staining of Lipids by the Periodic-Acid-Schiff Reaction. *Proc. Soc. Exp. Biol. Med.*, **75**, 583–585.
36. Bogoeva, B. and Petrusevska, G. (2001) Immunohistochemical and ultrastructural features of Gaucher's cells–five case reports. *Acta Med. Croatica*, **55**, 131–134.
37. Norman, R.M., Urich, H. and Lloyd, O.C. (1956) The neuropathology of infantile Gaucher's disease. *J. Pathol. Bacteriol.*, **72**, 121–131.
38. Bennett, S.A., Stevenson, B., Staines, W.A. and Roberts, D.C. (1995) Periodic acid-Schiff (PAS)-positive deposits in brain following kainic acid-induced seizures: relationships to fos induction, neuronal necrosis, reactive gliosis, and blood-brain barrier breakdown. *Acta Neuropathol.*, **89**, 126–138.
39. Sun, Y., Zhang, W., Xu, Y.-H., Quinn, B., Dasgupta, N., Liou, B., Setchell, K.D.R. and Grabowski, G.A. (2013) Substrate compositional variation with tissue/region and Gba1 mutations in mouse models–implications for Gaucher disease. *PLoS One*, **8**, e57560.
40. Lahiri, S. and Futerman, A.H. (2007) The metabolism and function of sphingolipids and glycosphingolipids. *Cell. Mol. Life Sci.*, **64**, 2270–2284.
41. Lloyd-Evans, E. (2003) Glucosylceramide and glucosylsphingosine modulate calcium mobilization from brain microsomes via different mechanisms. *J. Biol. Chem.*, **278**, 23594–23599.
42. Adachi, M., Wallace, B.J., Schneck, L. and Volk, B.W. (1967) Fine structure of central nervous system in early infantile Gaucher's disease. *Arch Pathol.*, **83**, 513–526.
43. Takahashi, K., Terashima, K., Hakozaki, H., Naito, M. and Kojima, M. (1978) Pathomorphology of lysosomal storage inclusions in the reticuloendothelial cells of sphingolipidosis. *Acta Histochem. Cytochem.*, **11**, 286–315.
44. Cervos-Navarro, J. and Zimmer, C. (1990) Light microscopic and ultrastructural study on CNS lesions in infantile Gaucher's disease. *Clin. Neuropathol.*, **9**, 310–313.
45. Korkotian, E., Schwarz, A., Pelled, D., Schwarzmann, G., Segal, M. and Futerman, A.H. (1999) Elevation of intracellular glucosylceramide levels results in an increase in endoplasmic reticulum density and in functional calcium stores in cultured neurons. *J. Biol. Chem.*, **274**, 21673–21678.
46. Farfel-Becker, T., Vitner, E., Dekel, H., Leshem, N., Enquist, I.B., Karlsson, S. and Futerman, A.H. (2009) No evidence for activation of the unfolded protein response in neuronopathic models of Gaucher disease. *Hum. Mol. Genet.*, **18**, 1482–1488.
47. Lieberman, A.P., Puertollano, R., Raben, N., Slaugenhaupt, S., Walkley, S.U. and Ballabio, A. (2012) Autophagy in lysosomal storage disorders. *Autophagy*, **8**, 719–730.
48. Osellame, L.D., Rahim, A.A., Hargreaves, I.P., Gegg, M.E., Richard-Londt, A., Brandner, S., Waddington, S.N., Schapira, A.H.V. and Duchen, M.R. (2013) Mitochondria and quality control defects in a mouse model of Gaucher disease-links to Parkinson's disease. *Cell Metab.*, **17**, 941–953.
49. Korschen, H.G., Yildiz, Y., Raju, D.N., Schonauer, S., Bonigk, W., Jansen, V., Kremmer, E., Kaupp, U.B. and Wachten, D. (2013) The Non-lysosomal-glucosidase GBA2 Is a Non-integral membrane-associated protein at the endoplasmic reticulum (ER) and golgi. *J. Biol. Chem.*, **288**, 3381–3393.
50. Meivar-Levy, I., Horowitz, M. and Futerman, A.H. (1994) Analysis of glucocerebrosidase activity using N-(1-[14C]hexanoyl)-D-erythroglucosylsphingosine demonstrates a correlation between levels of residual enzyme activity and the type of Gaucher disease. *Biochem. J.*, **303**, 377–382.
51. Bligh, E.G. and Dyer, W.J. (1959) A rapid method of total lipid extraction and purification. *Can. J. Biochem. Physiol.*, **37**, 911–917.
52. Shaner, R.L., Allegood, J.C., Park, H., Wang, E., Kelly, S., Haynes, C.A., Sullards, M.C. and Merrill, A.H. (2009) Quantitative analysis of sphingolipids for lipidomics using triple quadrupole and quadrupole linear ion trap mass spectrometers. *J. Lipid Res.*, **50**, 1692–1707.
53. Sullards, M.C., Liu, Y., Chen, Y. and Merrill, A.H. (2011) Analysis of mammalian sphingolipids by liquid chromatography tandem mass spectrometry (LC-MS/MS) and tissue imaging mass spectrometry (TIMS). *Biochim. Biophys. Acta*, **1811**, 838–853.